A Topology Optimization Based Design of Space Radiator for Focal Plane Assemblies

Xiao Shen [1,2] , Haitao Han [1,2] , Yancheng Li [1,2,3] , Changxiang Yan [2,4]* and Deqiang Mu [5]

1   Colledge of Materials Science and Opto-Electronic Technology, University of Chinese Academy of Sciences, Beijing 100049, China; hillbert2009@163.com (S.X.); haitaohan189@gmail.com (H.H.); 15802486979@163.com (Y.L.)
2   Changchun Institue of Optics, Fine Mechanics and Physics (CIOMP), Chinese Academy of Sciences, Changchun 130033, China
3   SKLAO, Changchun Institue of Optics, Fine Mechanics and Physics (CIOMP), Chinese Academy of Sciences, Changchun 130033, China
4   Center of Materials Science and Optoelectrics Engineering, University of Chinese Academy of Sciences, Beijing 100049, China
5   School of Mechanical and Electrical Engineering, Changchun University of Technology, Changchun 130033, China; mudq@ccut.edu.cn
*   Correspondence: yancx0128@126.com

Abstract: In this paper, to improve the heat dissipation efficiency of a radiator for focal plane assemblies, a topology optimization method is introduced into the design process. For the realization of the optimization, an objective of maximal thermal stiffness concerning the radiator is formulated. The topology optimization is performed under the same mass constraint of 2.05 kg as the initial design. To improve the manufacturability of topology optimization result, an inverse design is conducted to reconstruct a new model. In transient thermal simulation, the average maximal temperature on focal plane assemblies with a reconstructed radiator is 8.626 °C, while the average maximal temperature with the initial design is 9.793 °C. Compared to the initial design, a decrease of 1.167 °C on maximal temperature is achieved. As the heat dissipation efficiency of the proposed radiator design is improved compared to the initial design, it is meaningful in future applications.

Keywords: thermal design; optimization design; radiator; maximal thermal stiffness

1. Introduction

In space remote sensing, CCD(Charge-Coupled Device) and CMOS(Complementary Metal Oxide Semiconductor) are the most widely applied core photosensitive devices on space optical payloads due to their high definition and high quantum efficiency imaging, real-time data transmission and wide spectrum range [1]. These photosensitive components are quite sensitive to temperature, and excessive temperature fluctuation may worsen imaging quality by giving rise to dark current and thermal noise. For CCD, according to the research by Ahmad [2], a dark current would double itself when the temperature increases from 6 to 9 °C, for CMOS, the range is from 8 to 10 °C by Chen [3]. Generally, for CCD in space infrared remote sensors, the working temperature range shall be kept from −70 °C to −10 °C, and for the visible spectrum, the maximal upper limit can be 35 °C [4].

While in orbit, the thermal environment for remote sensors is serious: solar radiation, earth infrared radiation, earth albedo and space environment heat and cool the sensor alternatively. Considerable heat is generated when these power consuming assemblies are working. Since CCD and CMOS are small in size and of low heat capacity, excessive temperature fluctuations may easily occur if no reliable thermal control measures are taken.

Unlike ground devices which could dissipate heat through conduction or convection [5,6], in space, inner heat generation of CCD and CMOS would eventually be diffused into space through radiation. As a key part of the thermal control system of focal plane

assemblies, the design of the space radiators is a vital design task. To solve the design problem, an equivalent thermal resistance method [7–10] is widely used. With the method, the temperature of CCD assemblies would be determined in advance, then equivalent heat resistance for each part is evaluated to define the temperature of each part along the heat transfer path. Based on such estimation, the area of the radiator is evaluated. Finally, the validation of the design is done through CAE (Computer Aided Engineering) tools [2,7–10]. Although the heat resistance method has proven itself as a reliable tool, the engineering experience and thermodynamic calculation based classical method is time-consuming and the performance of the design relies heavily on the designer's experience. Furthermore, with complicated constraints, the improvement of heat dissipation efficiency on radiator design is hard to achieve. As in space observation, CCD and CMOS have strict requirements on working temperature, and the design problem is calling for new methods to improve heat dissipation efficiency.

In recent research concerning the optimization design of space radiators, most works are focused on large-scale radiators with a honeycomb structure [11–13]. In honeycomb radiator optimization designs, parameters such as the gap between every two adjacent heat pipes [13], thickness, or the materials and coating [12] are usually used as the optimization variations. The topology optimization method is also applied to determine the layout of heat tubes [11] in some cases. For radiators that work on miniaturized optical devices, due to strict installation and mass limits, a common solution is to use the outer cover of the optical device as the radiator [14]. In this case, it is feasible to improve the heat dissipation efficiency by optimizing material distribution of the outer cover based on the topology optimization method.

As a promising optimization design method, topology optimization, which is capable of systematically distributing materials in a certain domain under prescribed constraints, in recent years has become a popular optimization design method in structural engineering since its proposal in late 1980s by Bendsøe and Kikuchi [15]. Topology optimization is also effective in solving heat transferring problems, and many of the topology optimization techniques and methods are introduced and promoted in solving heat transfer optimization problems. Previous research is mainly focused on conduction and convection problems: J. Haslinger and A. Hillebrand [16] applied a homogenization method to optimize a heat conducting structure by controlling the variables represented by coefficients of elliptic equations; Bendsøe [17] and C.Seonho [18] introduced the SIMP [19] (Solid Isotropic Material with Penalization) method into heat conduction problems; A.Iga [20] summarized the topology optimization process of the problems concerning thermal conduction and convection with design-dependent effects; Alexandersen [21] proposed an optimization with a large scale three-dimensional sink under natural convection; Li [22,23] and Xie [24] dealt with heat conduction problems with the ESO (Evolutionary Structural Optimization) method [23].

Concerning optimization design problems with radiation boundary, the research is quite minimal. For the design of a radiative enclosure, D.A. Castro [25] calculated a design-dependent view factor between the radiating surfaces and discussed two objectives, aiming at maximizing the net flux and minimizing the temperature summation. Through topology optimization, Castro changed the maximal temperature from 845.97 to 800.98 °C. The radiative enclosure is simplified into a two-dimensional plane model, and only radiation is considered in the optimization. In Fan's research [11], a two step optimization is done to strengthen the heat dissipation efficiency of a large-scale butterfly wing radiator. The optimization decreases 73.4 °C on maximal temperature under a uniform heat source. In the first step, the shape of the radiator is selected from many Pareto solutions, the objective represents a weighted combination of heat dissipation per mass and temperature differences at boundary points. Then in the second step, the heat tube layout is decided by a topology optimization only based on mean compliance concerning heat conduction. For the radiator discussed in this paper, since the material is homogeneous and the heat conduction and radiation of the radiator are coupled, the objective of the topology optimization should be

able to describe the influences of both conduction and radiation, which is seldom discussed in previous research.

In this paper, to improve the heat dissipation efficiency of a radiator that works for focal plane assemblies on a miniaturized space optical device, topology optimization is introduced into the design process. For realization of topology optimization, an objective based on maximal thermal stiffness concerning radiators is formulated. After reconstructing the radiator based on the topology optimization result, the final design could be validated through transient simulation. Simulation results indicate that after topology optimization, the maximal temperature of CCD assemblies is decreased by 1.167 °C. The reconstructed radiator design optimized the material distribution under prescribed constraints, which is meaningful in future applications.

2. Thermal Analysis of the Radiator Design Problem

2.1. Thermal Environment of the Radiator

While in orbit, the thermal environment [26,27] for space radiators is complicated, e.g., inner heat generation by CCD components, heat exchange with the space environment. In the mean time, the radiator may also absorb heat from possible external heat flow, e.g., solar radiation, earth radiation, and earth albedo, as shown in Figure 1.
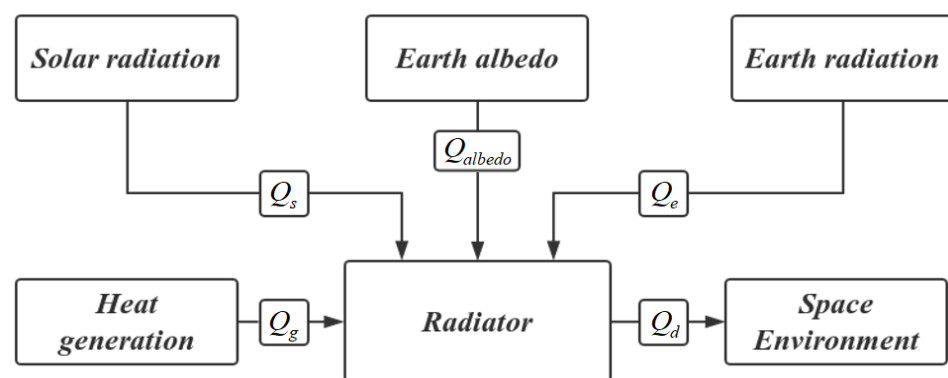

Figure 1. Thermal environment of the radiator.

When working in space, a set equations concerning thermal fluxes [26,28] for radiators can be listed as follows:

$$\begin{cases} Q_s = \alpha_s F_s E_s A \\ Q_e = \varepsilon_h F_e E_e A \\ Q_{albedo} = \alpha_s F_a k_{albedo} E_s A \\ Q_g = \sum q_j A_j \\ Q_d = \varphi \varepsilon \sigma (T_a^4 - T^4) A \\ Q_t = mC \frac{\partial T}{\partial t} \end{cases} \tag{1}$$

where q_j refers to the flux conducted to the radiator by heat pipe, or flexible thermal strap, and A_j refers to the area that each heat flux go through. According to the first law of thermodynamics, the radiator equation below is satisfied

$$Q_t + Q_d = Q_g + Q_{albedo} + Q_e + Q_s \tag{2}$$

2.2. Generalization of the Governing Equations and Boundaries of Radiator Design Problems

In this section, a certain radiator is transformed into a generalized model. As shown in Figure 2, q_1 refers to the heat flux conducted by heat pipe or flexible thermal strap-on boundary Γ_1. On Γ_2, q_2 refers to the net flux radiating into the space environment. For domain Ω, Γ is the outer boundary, given by $\Gamma = \Gamma_1 \cup \Gamma_2 \cup \Gamma_{dir}$, and Γ_{dir} refers to the insulation boundary.
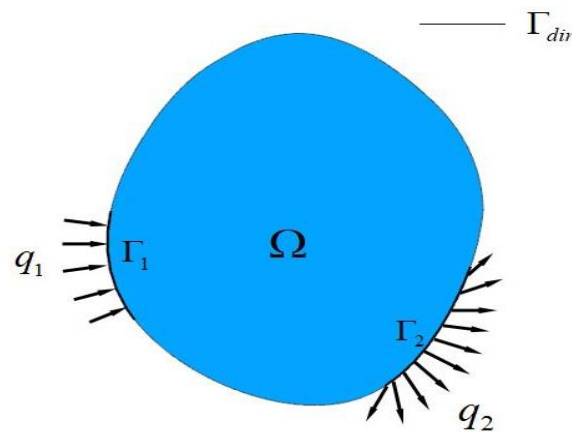
Figure 2. Generalization of the thermal radiation problem.

Within domain Ω, for radiator design problems, the governing equation is as follows:

$$\frac{\partial}{\partial x}(k_x \frac{\partial T}{\partial x}) + \frac{\partial}{\partial y}(k_y \frac{\partial T}{\partial y}) + \frac{\partial}{\partial z}(k_z \frac{\partial T}{\partial z}) = 0 \tag{3}$$

As what has been depicted in Figure 2, the whole boundary Γ, which is the total outer boundary of domain Ω, is split into different subsets, and for each part, equations concerning different heat fluxes are as follows:
on Γ_{dir}:

$$q_{dir} = 0 \tag{4}$$

on Γ_1:

$$q_1 = -(k_x \frac{\partial T}{\partial x} n_x + k_y \frac{\partial T}{\partial y} n_y + k_z \frac{\partial T}{\partial z} n_z) \tag{5}$$

$$Q_g = \iint\limits_{\Gamma_1} q_1 ds \tag{6}$$

where q_1 is the prescribed heat flux, n_x, n_y, n_z is the direction cosine between q_1 and coordinate axises x, y, z.
on Γ_2:

$$q_2 = \alpha_s F_s E_s + \varepsilon_h F_e E_e + \alpha_s F_a k_{albedo} E_s + \varphi \varepsilon_h \sigma T_a^4 - \varphi \varepsilon_h \sigma T^4 \tag{7}$$

$$\iint\limits_{\Gamma_2} q_2 ds = Q_s + Q_e + Q_{albedo} + Q_d \tag{8}$$

3. Formation of the Topology Optimization Model

In this section, a topology optimization model concerning the radiator is explained, including the SIMP interpolation model and the objective. The work flow of the whole optimization design process is also illustrated.

3.1. SIMP Model

One key idea of the topology optimization method is the introduction of a certain fixed design domain Ω that includes the optimized domain Ω_0, and the artificial density function χ below is satisfied within the domain:

$$\chi(x,y,z) = \begin{cases} 1, & if \quad (x,y,z) \in \Omega \\ 0, & if \quad (x,y,z) \in \Omega \setminus \Omega_0 \end{cases} \tag{9}$$

where (x,y,z) denotes the position in domain Ω.

With Function (9), the structural design problem is transferred into a problem of solving material distribution problems incorporated with an interpolated characteristic function. As this function is highly discontinuous, a smoothing technique is introduced: the well-known SIMP model [19]. The SIMP model of element thermal conductivity can be expressed as:

$$k_i = k_{imin} + \chi_l^p (k_{i0} - k_{imin}), i = x, y, z \tag{10}$$

where k_{i0} is the original thermal conductivity of the given material. To avoid singularity during iterations, the parameter k_{imin} is set as the lower bound of the thermal conductivity. The variation χ_l is a continuous variation named artificial density, l represents the number of the element. Parameter p is a penalty, which forces k_i to approach either k_{imin} or k_{i0}. The volume integration concerning the density satisfies the following inequality:

$$\sum_l \chi_l v_e = \iiint_\Omega \chi(x, y, z) dv \le V, 0 \le \chi(x, y, z) \le 1. \tag{11}$$

Allowing for radiation on boundary of Γ_2, some parameters may also need to be interpolated as follows:

$$\begin{cases} \varepsilon_{hi} = \varepsilon_{hmin} + \chi_l^p (\varepsilon_{h0} - \varepsilon_{hmin}) \\ \alpha_{si} = \alpha_{smin} + \chi_l^p (\alpha_{s0} - \alpha_{smin}) \end{cases} \tag{12}$$

where ε_{hmin} is the prescribed minimal value of emittance that avoids the singularity during iterations, ε_{h0} is the given emittance of surface Γ_2, α_{smin} is the prescribed minimal value of absorptance, and α_{s0} is the given absorptance of surface Γ_2.

3.2. Formation of the Optimization Objective

In this section, the objective of maximal thermal stiffness concerning radiators aiming at maximizing the thermal diffusivity [20] is formed.

An appropriate objective is vital for an optimization design. Since in space observation, most photosensitive devices work intermittently, a perfect radiator design shall guarantee that in each working cycle, the temperature fluctuation is kept in a minimal range. Therefore, a rational description of the problem can be as follows: to find a structure that has the least temperature rise after transferring a prescribed quantity of heat. In analogy with maximal structural stiffness [29] in usual mechanical problems, for radiators under the same constraints and loads, the most effective design should have the maximal "thermal stiffness".

Previously for optimization problems concerning conduction and convection, an objective based on the concept of total potential energy [20], aiming at maximizing the thermal diffusivity, or in another way maximizing thermal stiffness, is widely applied. As by T. E. Bruns [30], the boundary of radiation can be calculated as a kind of nonlinear convection, referring to the idea applied in previous conduction and convection optimization research, and an objective of maximal thermal stiffness concerning a radiation boundary is formed.

Suppose u as the virtual temperature field, through the principle of virtual temperature [31] and integration by parts, a weak form of Equation (3) could be put as follows:

$$\iiint_\Omega \left(\frac{\partial u}{\partial x} k_x \frac{\partial T}{\partial x} + \frac{\partial u}{\partial y} k_y \frac{\partial T}{\partial y} + \frac{\partial u}{\partial z} k_z \frac{\partial T}{\partial z} \right) dv - \iint_\Gamma \left(k_x \frac{\partial T}{\partial x} n_x + k_y \frac{\partial T}{\partial y} n_y + k_z \frac{\partial T}{\partial z} n_z \right) u ds = 0 \tag{13}$$

Substituting all boundaries in Equations (4), (5), (7) and (13) could be transformed into the form below:

$$a(T, u) = L(u) \tag{14}$$

where $a(T, u)$ on the left-hand side is given by

$$a(T, u) = \iiint\limits_{\Omega} (\frac{\partial u}{\partial x} k_x \frac{\partial T}{\partial x} + \frac{\partial u}{\partial y} k_y \frac{\partial T}{\partial y} + \frac{\partial u}{\partial z} k_z \frac{\partial T}{\partial z}) dv \tag{15}$$

$L(u)$ on the right-hand is given by

$$L(u) = \iint\limits_{\Gamma_2} (\alpha_s F_s E_s + \alpha_e F_e E_e + \varepsilon_h F_a E_a + \varphi \varepsilon_h \sigma T_a^4) u ds + \iint\limits_{\Gamma_1} q_1 u ds - \iint\limits_{\Gamma_2} \varphi \varepsilon T^4 u ds \tag{16}$$

Through the variational operation, the objective function of total potential energy, or in another way the function of maximal thermal stiffness, can be expressed as follows:

$$G(\chi) = \frac{1}{2} a(T, T) - \frac{3}{10} \iint\limits_{\Gamma_2} T \varphi \varepsilon_h \sigma T_a^4 ds - L(T) \tag{17}$$

where $\frac{3}{10} \iint\limits_{\Gamma_2} T \varphi \varepsilon_h \sigma T_a^4 ds$ in the equation represents the revisional term to the nonlinear radiation boundary.

3.3. Finite Element Solution of the Problem

In this section, the FEM (Finite Element Method) is applied to discretize and calculate the temperature field. Thru FEM, the continuous temperature field T of a certain element would be transformed into an interpolation model as follows:

$$T = \mathbf{N}\mathbf{T}_e \tag{18}$$

where $\mathbf{N}$ refers to the shape function, defined as $\mathbf{N} = [N_1, N_2, \cdots, N_n]$, $\mathbf{T}_e$ refers to nodal temperature vector, given by $\mathbf{T}_e = [T_1, T_2, \cdots, T_n]^T$.

Within domain Ω and all its boundaries, through the Galerkin method, the governing equation is Equation (4), and the boundaries are Equations (6) and (8), which can finally be discretized as a FEM equation below:

$$\mathbf{K}_{con}\mathbf{T} + \mathbf{K}_{rad}\mathbf{T} = \mathbf{P} \tag{19}$$

where $\mathbf{K}_{con}\mathbf{T}$ represents the contribution of the conduction within the domain to the FEM equilibrium, $\mathbf{K}_{rad}\mathbf{T}$ refers to the contribution of radiation on Γ_2, and $\mathbf{P}$ is the global thermal load vector, consisting of several different parts: inner heat generation by focal plane components, possible external radiation load from the solar radiation, earth radiation, and earth albedo.

3.4. Formation of Mathematical Model

In this section, the mathematical model of the optimization problem is elaborated. By substituting Equation (19), the problem for maximization of the thermal stiffness under a certain volume constraint can be formulated as:

$$\begin{aligned} &Maximize \quad G(\chi) \\ &G(\chi) = \frac{1}{2} a(T, T) - \frac{3}{10} \iint\limits_{\Gamma_2} T \varphi \varepsilon_h \sigma T_a^4 ds - L(T) \\ &\qquad\quad = -\frac{1}{2} \mathbf{T}^T \mathbf{K}_{con} \mathbf{T} - \frac{4}{5} \mathbf{T}^T \mathbf{K}_{rad} \mathbf{T} \\ &s.t. \\ &\qquad \iiint\limits_{\Omega} \chi dv \leq V \\ &\qquad \mathbf{K}_{con}\mathbf{T} + \mathbf{K}_{rad}\mathbf{T} = \mathbf{P} \end{aligned} \tag{20}$$

More often, this problem is transformed into an equivalent function, given by:

$$
\begin{aligned}
&Minimize \quad F(\chi) \\
&F(\chi) = \tfrac{1}{2}\mathbf{T}^T\mathbf{K}_{con}\mathbf{T} + \tfrac{4}{5}\mathbf{T}^T\mathbf{K}_{rad}\mathbf{T} \\
&s.t. \\
&\qquad \iiint\limits_{\Omega} \chi dv \leq V \\
&\qquad \mathbf{K}_{con}\mathbf{T} + \mathbf{K}_{rad}\mathbf{T} = \mathbf{P}
\end{aligned}
\tag{21}
$$

3.5. Optimization Design Work Flow

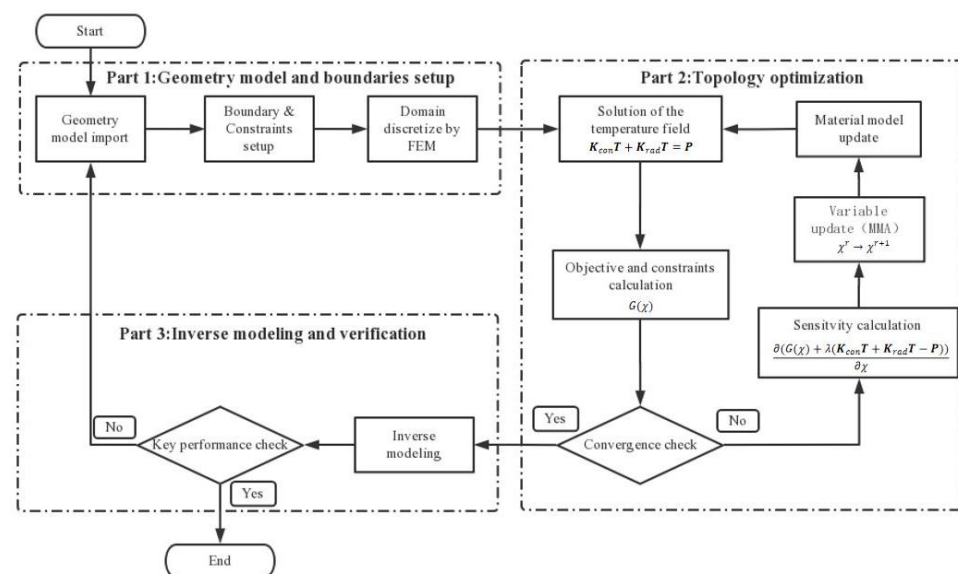The flowchart for the whole optimization design is shown in Figure 3:

Figure 3. Work flow of the optimization design.

The total work flow consists of three parts: the geometry model and boundaries setup, topology optimization, and an inverse design based on the results of the topology optimization and the verification.

The first part is the geometry model and boundaries setup, including configurations of the geometry model of the optimization domain, constraints and boundaries. In this procedure, an equivalent thermal resistance method is used to form an initial design.

In the second part, firstly Equation (19) is solved to obtain the global nodal temperature vector **T**. Then, the objective and all other constraints are evaluated and convergence is checked:

$$
\left| \frac{max(\chi^{r+1}) - max(\chi^r)}{max(\chi^r)} \right| \leq \varepsilon_u
\tag{22}
$$

where $max(\chi^r)$ represents the maximal χ_l at iteration r, and ε_u is the convergence tolerance. In the iterations, updates by MMA (Method of Moving Asymptotes) [32] of each χ_l and **T** are continued until the convergence is met.

Since most topology optimization may have structures of low fabricability, in the third part, some simplifications are done through an inverse modeling to reconstruct the radiator. Then, key performance tests of the reconstructed design are conducted. If some key indicators are not met, the design process would restart from the first part and end when the reconstructed radiator can meet all requirements.

4. Optimization Design of the Radiator

In this section, the radiator design problem is solved by topology optimization, and both results of initial design by the thermal resistance method and the reconstructed model are compared.

4.1. Initial Design of the Radiator

The radiator is designed for focal plane assemblies of a space camera. In Figure 4, the main components of the heat dissipation system of CCD assemblies are revealed. Along the heat transferring path, total thermal resistance R_{total} consists of the following parts: R_1, R_3, R_5 and R_7, each represents the contact thermal resistance between every two adjacent components. R_2 refers to equivalent thermal resistance of the gasket, R_4 represents the resistance of the aluminum sink, and R_6 represents the thermal resistance of the thermal strap.
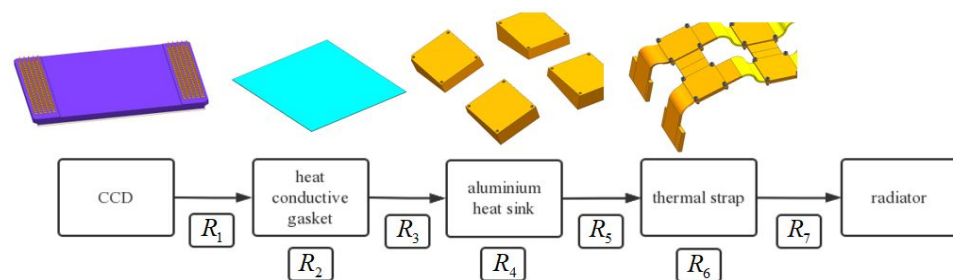

Figure 4. Components along the heat transfer path.

In Table 1, parameters of the materials are shown, and silver foil and heat conductive grease are materials used for the filler.

Table 1. Parameters of the materials

Material	Conductivity (W/(m · K))	Density (kg/m³)	Specific Heat Capacity (J/(kg · K))
Aluminum	155	2700	900
Heat conductive gasket	3.5	/	/
Silver foil	400	10,530	230
Heat conductive grease	1.5	/	/

While operating on orbit, the total power consumption of CCD assemblies is $P_{load} = 16\ W$, and the load is conducted to the radiator through fours channels equally. As the permissible working temperature range for each CCD is 0∼25 °C, allowing for some redundancy, the maximal working temperature is set as $T_{pre} = 20$ °C.

Through the equivalent thermal resistance method, the total radiating area is calculated as below:

$$A_{eva} = \frac{P_{load}}{\varepsilon \sigma ((T_{pre} - \Delta T)^4 - T_a{}^4)} = 0.051\ \text{m}^2 \tag{23}$$

where ΔT refers to the temperature decrease along the heat transfer path, given by $\Delta T = \frac{P_{load}}{R_{total}}$, the total resistance R_{total} is given by $R_{total} = R_1 + R_2 + \cdots + R_7$.

Allowing for actual installation and motion limits, the back cover in Figure 5 is designed as the space radiator, and the material of the cover is aluminum. The thickness is set as 0.003 m. On the radiator, the area each inflow heat flux goes through is 0.012 m² = 0.03 m × 0.04 m.
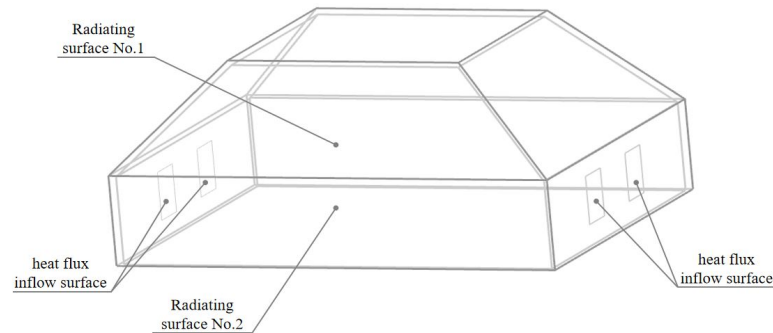
Figure 5. Initial design of the radiator.

Two areas on the radiator, each named No. 1 and No. 2, are assigned to radiate heat into the space. The view factor is 1 for surface No. 2, and 0.85 for surface No. 1, allowing for the blockage by surrounding supports. The area is 0.0286 m^2 for surface No. 1 and 0.0285 m^2 for surface No. 2. Both surfaces are coated with KSZ coating, whose emissivity is $\varepsilon = 0.9$. The results of the steady state thermal simulation of the initial design are shown in Table 2. As 2.05 kg is the weight upper limit of this cover, the weight meets the requirement.

Table 2. Results of steady thermal simulation of the initial design.

Load (W)	Maximal Temperature (°C)	Minimal Temperature (°C)	Weight (kg)
16	18.231	1.645	2.026

In Figure 6, the maximal temperature and the isothermal surface are illustrated.
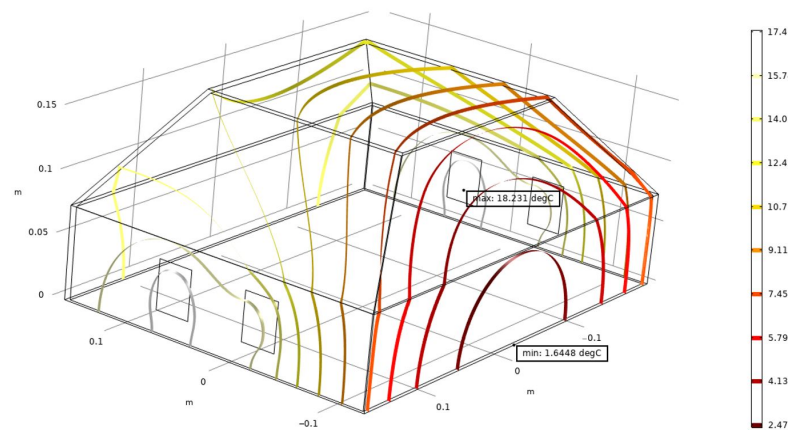

Figure 6. Isothermal surface of initial design under steady thermal state.

4.2. Mesh Configuration

Sharp corners of the cover could result in overdense meshes. Furthermore, compared to the remaining parts of the cover, these corners are of much smaller volume and superficial area, which means corners contribute much less to the whole heat transfer process than the rest of the parts. In this case, to avoid complicated calculation on these dense meshes in topology optimization, a particular mesh procedure is done. The cover is divided into two parts, one part as the optimization domain, and the other is the maintenance domain, only involved in turning heat flow. The mesh for the two respective domains is shown in Figure 7.
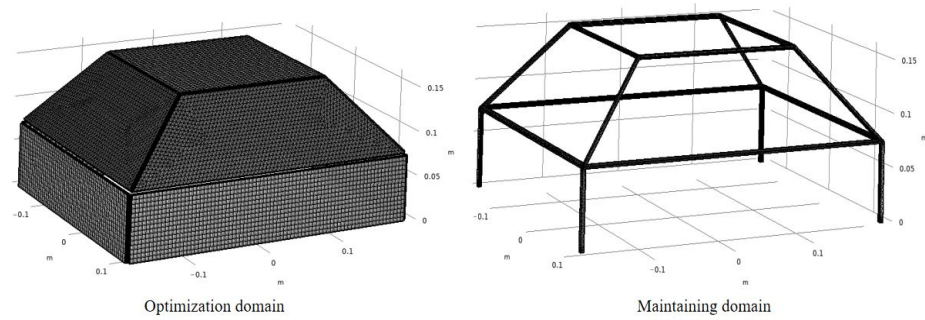
Figure 7. Mesh configuration of the cover.

As shown in Figure 8, allowing for essential thickness to shield the electromagnetic interference [33], in the optimization domain, the artificial density variables χ_l of two layers of elements are prescribed as one.
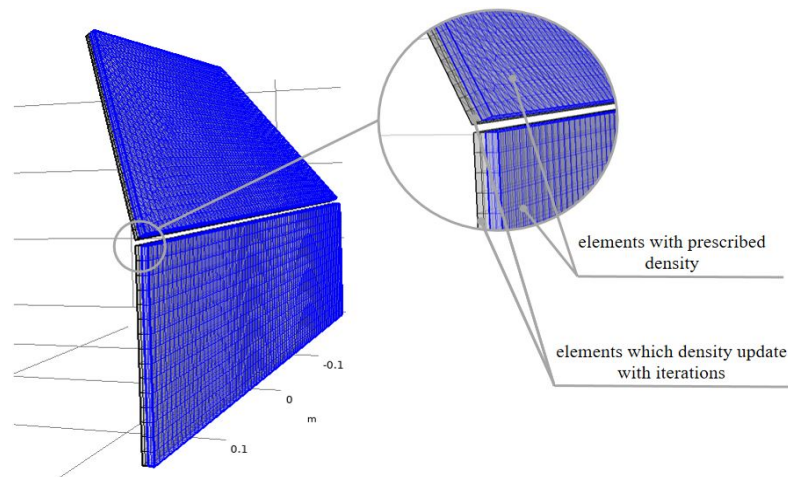

Figure 8. Optimization domain with different artificial density.

4.3. Topology Optimization Result of Maximal Thermal Stiffness Design

Material distribution of the radiator after topology optimization is shown in Figure 9, the color stripe represents the temperature for each isothermal surface.
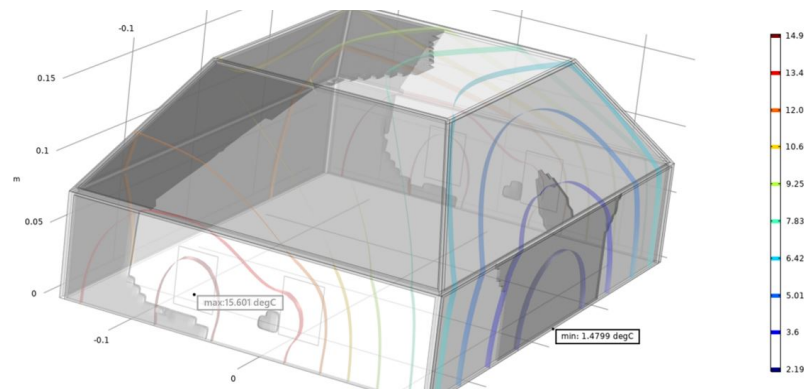

**Figure 9.** Material distribution of topology optimization result.

In Table 3, the results of the steady state thermal simulation is shown, and compared to the initial design in Section 4.1, a decrease of 2.63 °C of the maximal temperature on the radiator is achieved.

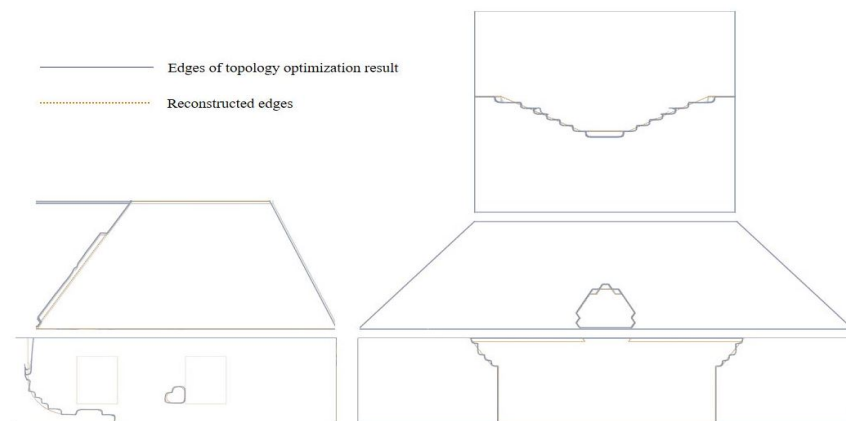**Table 3.** Results of the steady state thermal simulation of the radiator after topology optimization.

Load (W)	Maximal Temperature (°C)	Minimal Temperature (°C)	Weight (kg)
16	15.601	1.480	2.048

4.4. Reconstruction of the Radiator

Since topology optimization result has complicated edges, to improve manufacturability, an inverse modeling based on the topology optimization result is conducted. As shown in Figure 10, the complicated zigzag edges of the optimized model are replaced by smooth curves and straight lines.
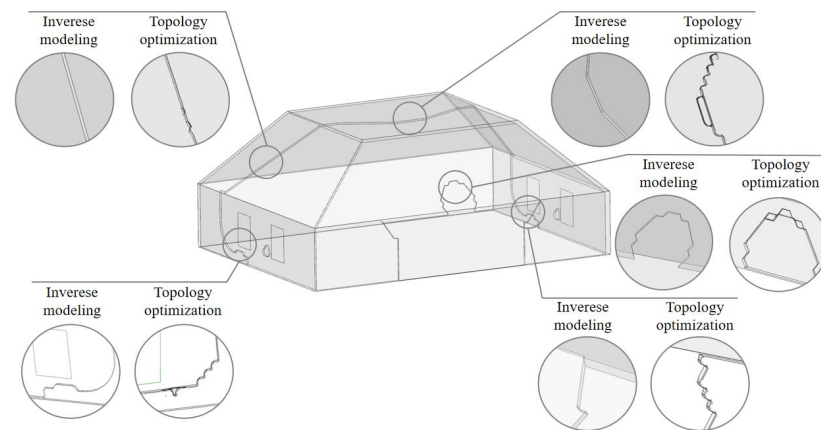
Figure 10. Simplifications.

The construction follows such principles: (1) Total weight of the reconstructed radiator must not exceed the weight limit of 2.05 kg. (2) Complicated edges on the radiator need to be replaced by straight or curve edges, which are of better manufacturability, and after construction, the area of each surface needs to be kept roughly the same, as shown in Figure 11.

Figure 11. Reconstruction of the complicated edges.

After reconstruction, the same steady state thermal simulation is applied to the reconstructed radiator. The results are shown in Figure 12.
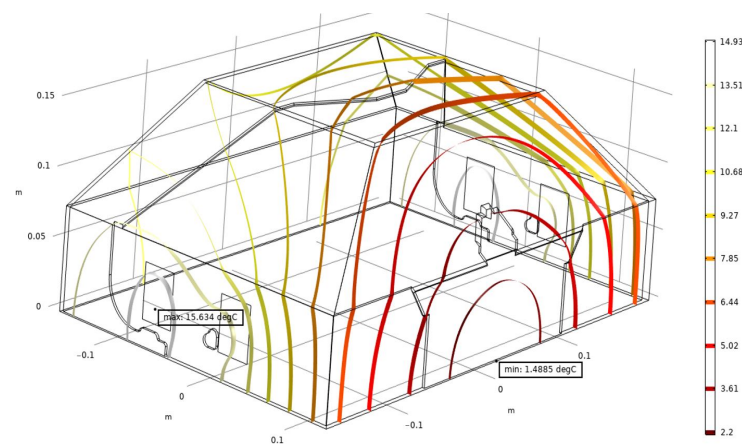
Figure 12. Steady thermal simulation of the reconstructed radiator.

As shown in Table 4, the simulation results of the three designs are illustrated, and compared to topology optimization results, the max temperature on the reconstructed radiator is 0.033 °C higher. The constructed radiator maintains a decrease of 2.597 °C on max temperature compared to the initial radiator.

Table 4. Steady state simulation results of the three designs.

Design	Max Temperature (°C)	Min Temperature (°C)	Weight (kg)
Initial design	18.231	1.645	2.011
Topology optimization	15.601	1.480	2.048
Reconstructed radiator	15.634	1.489	2.029

4.5. Transient Thermal State Simulation

As CCD assemblies work periodically, the scrutiny of transient thermal performance of the radiator is also essential.

In transient simulation, both systems with the initial radiator and reconstructed radiator are tested under the same orbital working conditions: each working cycle contains a working duration of 1500 s and a shutdown duration of 2100 s. In working durations, the total power consumption of CCD assemblies is 16*W*, and in shutdown durations, extra active temperature compensation measures are taken to avoid CCD assemblies being overcooled.

4.6. Results

Figure 13 reveals the transient temperature rising curves of CCD assemblies in five working cycles.

As shown in Table 5, the average maximal temperature on CCD with the reconstructed radiator is 8.626 °C, while the temperature is 9.793 °C with the initial design. An average decrease of 1.167 °C on CCD is achieved with the reconstructed radiator.

Table 5. Maximal temperature of CCD assemblies in working cycles for both systems.

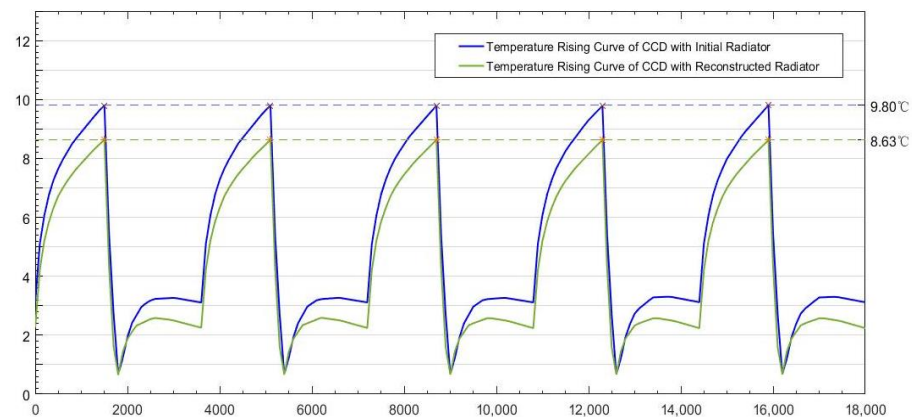| Time (s)	1500	5100	8700	12,300	15,900
Max temperature on CCD with initial radiator (°C)	9.793	9.792	9.787	9.787	9.805
Max temperature on CCD with reconstructed radiator (°C)	8.634	8.627	8.629	8.620	8.619

Figure 13. Temperature rising curves on CCD of both systems.

5. Conclusions

To improve the heat dissipation efficiency of a radiator for CCD assemblies of a miniaturized space optical device, a topology optimization method is introduced into the radiator design process. To accomplish the optimization design, a special objective function is formed, and inverse modeling is applied to improve the manufacturability. Finally, the transient thermal state simulation validates the design. In the process, the results below were obtained:

(1) The objective of maximal thermal stiffness formed in this paper could describe influences of coupled conduction and radiation on the radiator.

(2) Inverse modeling based on the result of topology optimization could improve manufacturability. As the maximal temperature on reconstructed radiator increases by 0.033 °C compared to topology optimization result, the heat dissipation efficiency improvement by topology optimization could be retained to a great extent after reconstruction.

(3) The transient simulation results indicate that heat dissipation efficiency is improved on reconstructed radiator, as an average decrease of 1.167 °C of maximal temperature on CCD assemblies in working durations is achieved compared to those with initial radiator. The improvement makes a longer working duration per cycle possible under the same temperature limits.

Author Contributions: Conceptualization, X.S.; methodology, X.S. and H.H.; software, X.S.; validation, X.S., H.H. and Y.L.; formal analysis, X.S., H.H. and Y.L. ; investigation, X.S.; resources, X.S.; data curation, X.S.; writing—original draft preparation, X.S.; writing—review and editing, X.S., H.H. and Y.L.; visualization, X.S.; supervision, C.Y. and D.M.; project administration, C.Y.; funding acquisition, C.Y. All authors have read and agreed to the published version of the manuscript.

Institutional Review Board Statement: Not applicable.

Informed Consent Statement: Not applicable.

Data Availability Statement: Not applicable.

Conflicts of Interest: The authors declare no conflict of interest.

Nomenclature

Q_s	solar radiation absorption
Q_e	earth radiation absorption
Q_{albedo}	albedo absorption
Q_g	external heat flow generated by power-consuming sensors
Q_d	the energy that radiating into space environment
Q_t	time dependent energy change within the radiator
α_s	solar radiation absorptance
F_s	view factor of solar radiation
E_s	solar constant
α_e	earth radiation absorptance
F_e	view factor of earth radiation
E_e	earth radiation
F_a	view factor of albedo
A	area of the radiator
k_x,k_y,k_z	isotropical thermal conductivity
k_{albedo}	earth albedo
φ	view factor of the radiating surface to the space
ε_h	hemispherical emittance
σ	Stefan–Boltzmann constant
Γ	outer surface of the domain
T_a	ambient temperature
λ	Lagrange multiplier
Ω	optimization domain
T	temperature field on radiator
C	specific heat capacity
ρ	density
m	mass of the radiator
t	time
n	number of element nodes
$\mathbf{T}_e$	element nodal temperature vector
$\mathbf{K}_{con}$	global heat conduction matrix
$\mathbf{K}_{rad}$	global thermal radiation matrix
$\mathbf{T}$	nodal temperature vector
$\mathbf{P}$	global thermal load vector
χ	artificial density
u	virtual temperature
$G(\chi)$	objective function of max thermal stiffness
$F(\chi)$	equivalent objective function
P_{load}	thermal load
T_{pre}	prescribed working temperature
R_{total}	total thermal resistance
p	penalty

References

1. Xu, X.; Li, Z.; Xue, L. Analysis and processing of CCD noise. *Infrared Laser Eng.* **2004**, *33*, 343–357.
2. Ahmad, A.; Arndt, T.; Gross, R.; Hahn, M.; Panasiti, M. Structural and thermal modeling of a cooled CCD camera. *Proc. SPIE Int. Soc. Opt. Eng.* **2001**, *4444*, 122–129.
3. Jian, C. Research of CMOS Image Sensor. *Electron. Sci. Technol.* **2007**, *144*, 73–76.
4. Chen, L.H.; Li, Y.C.; Luo, Z.T.; Dong, J.H.; Wang, Z.S.; Xu, S.Y. Thermal design and testing of CCD for space camera. *Opt. Precis. Eng.* **2011**, *19*, 2117–2122. [CrossRef]
5. Sarafraz, M.M.; Dareh Baghi, A.; Safaei, M.R.; Leon, A.S.; Ghomashchi, R.; Goodarzi, M.; Lin, C.-X. Assessment of Iron Oxide (III)–Therminol 66 Nanofluid as a Novel Working Fluid in a Convective Radiator Heating System for Buildings. *Energies* **2019**, *12*, 4327. [CrossRef]
6. Bagherzadeh, S.A.; Jalali, E.; Sarafraz, M.M.; Akbari, O.A.; Karimipour, A.; Goodarzi, M.; Bach, Q.-V. Effects of magnetic field on micro cross jet injection of dispersed nanoparticles in a microchannel. *Int. J. Numer. Methods Heat Fluid Flow* **2019**, *30*, 2683–2704.

7. Han, D.; Wu, Q.W.; Lu, E.; Chen, L.H.; Yang, C.Y. Thermal design of CCD focal plane assemblies for attitude-varied space cameras. *Opt. Precis. Eng.* **2009**, *17*, 2665–2671.

8. Chen, E.T.; Lu, E.; Chen, L.H.; Yang, C.Y. Thermal engineering design of CCD component of space remote-sensor. *Opt. Precis. Eng.* **2000**, *8*, 523–526.

9. Wu, Q.W.; Guo, L. Thermal design and proof tests of CCD components in spectral imagers. *Opt. Precis. Eng.* **2009**, *17*, 2441–2444.

10. Zi, K.M.; Wu, Q.W.; Guo, J.; Luo, Z.T.; Chen, L.H.; Li, M. Thermal design of CCD focal plane assembly of space optical remote-sensor. *Opt. Tech.* **2008**, *34*, 401–407.

11. Fan, G.; Duan, B.; Zhang, Y.; Ji, X.; Qian, S. Thermal control strategy of OMEGA SSPS based simultaneous shape and topology optimization of butterfly wing radiator. *Int. Commun. Heat Mass Transf.* **2020**, *119*, 104912. [CrossRef]

12. da Silva, D.F.; Muraoka, I.; de Sousa, F.L.; Garcia, E.C. Multiobjective and Multicase Optimization of a Spacecraft Radiator. *J. Aerosp. Technol. Manag.* **2019**, *11*, e0518. [CrossRef]

13. Kim, T.Y.; Chang, S.Y.; Yong, S.S. Optimizing the Design of Space Radiators for Thermal Performance and Mass Reduction. *J. Aerosp. Eng.* **2016**, *30*, 04016090. [CrossRef]

14. Jiang, F.; Wu, Q.; Wang, Z.; Liu, J.; Deng, H. Thermal design and analysis of high power star sensors. *Case Stud. Therm. Eng.* **2015**, *6*, 52–60. [CrossRef]

15. Bendsøe, M.P.; Noboru, K. Generating optimal topologies in structural design using a homogenization method. *Comput. Methods Appl. Mech. Eng.* **1998**, *71*, 197–224. [CrossRef]

16. Haslinger, J.; Hillebrand, A.; Kärkkäinen, T.; Miettinen, M. Optimization of conducting structures by using the homogenization method. *Struct. Multidiscip. Optim.* **2002**, *24*, 125–140. [CrossRef]

17. Bendsøe, M.P. Optimal shape design as a material distribution problem. *Struct. Optim.* **1989**, *1*, 193–202. [CrossRef]

18. Cho, S.; Choi, J.Y. Efficient topology optimization of thermo-elasticity problems using coupled field adjoint sensitivity analysis method. *Finite Elem. Anal. Des.* **2005**, *41*, 1481–1495. [CrossRef]

19. Bendsøe, M.; Sigmund, O. *Topology Optimization—Theory, Methods and Applications*; Springer: Berlin/Heidelberg, Germany, 2003; pp. 2–62.

20. Iga, A.; Nishiwaki, S.; Izui, K.; Yoshimura, M. Topology optimization for thermal conductors considering design-dependent effects, including heat conduction and convection. *Int. J. Heat Mass Transf.* **2009**, *52*, 2721–2732. [CrossRef]

21. Joe, A.; Ole, S.; Niels, A. Large scale three-dimensional topology optimisation of heat sinks cooled by natural convection. *Int. J. Heat Mass Transf.* **2016**, *100*, 876–891.

22. Yin, L.; Ananthasuresh, G.K. A novel topology design scheme for the multi-physics problems of electro-thermally actuated compliant micromechanisms. *Sens. Actuators A Phys.* **2009**, *97*, 599–609.

23. Xie, Y.M.; Steven, G.P. *Evolutionary Structural Optimization*; Springer: Lodon, UK, 1997; pp. 12–61.

24. Qing, L.I.; Steven Grant, P.; Querin Osvaldo, M. Shape and topology design for heat conduction by Evolutionary Structural Optimization. *Int. J. Heat Mass Transf.* **1999**, *42*, 3361–3371.

25. Castro, D.A.; Kiyono, C.Y.; Silva, E.C.N. Design of radiative enclosures by using topology optimization. *Int. J. Heat Mass Transf.* **2015**, *88*, 880–890. [CrossRef]

26. Ming, G.R.; Guo, S. *Thermal Control of Spacecraft*, 2nd ed.; Science Press: Beijing, China, 1998; pp. 5–56.

27. Gunga, H.C.; Steinach, M.; Werner, A.; Kirsch, K.A. *Handbook of Space Technology*; Wiley: West Sussex, UK, 2009; pp. 33–51.

28. Yang, S.M.; Tao, W.Q. *Heat Transfer*, 4th ed.; Beijing Higher Education Press: Beijing, China, 1998; pp. 20–118.

29. Niu, F.; Xu, S.L.; Cheng, G.D. A general formulation of structural topology optimization for maximizing structural stiffness. *Struct. Multidipl. Optim.* **2011**, *43*, 561–572. [CrossRef]

30. Bruns, T.E. Topology optimization of convection-dominated, steady-state heat transfer problems. *Int. J. Heat Mass Transf.* **2007**, *50*, 2859–2873. [CrossRef]

31. Qi, Y.; He, Y.; Zhang, W.; Guo, J. Thermal analysis and design of electronic equipments. *Mod. Electron. Technol.* **2003**, *144*, 73–76.

32. Svanberg, K. The method of moving asymptotes—A new method for structural optimization. *Int. J. Numer. Methods Eng.* **2010**, *24*, 359–373. [CrossRef]

33. Sophie, D. Radiation effects on electronic devices in space. *Aerospaceence Technol.* **2005**, *9*, 93–99.